FRONTIERS OF PHYSICS

RESEARCH ARTICLE
Volume 19 / Issue 3 / 33211 / 2024

Localization–delocalization transitions in non-Hermitian Aharonov–Bohm cages

Xiang Li*, Jin Liu*, Tao Liu†

School of Physics and Optoelectronics, South China University of Technology, Guangzhou 510640, China
*These authors contributed equally to this work.
Corresponding author. E-mail: †liutao0716@scut.edu.cn
Received March 12, 2024; accepted April 10, 2024

ABSTRACT

A unique feature of non-Hermitian systems is the extreme sensitivity of the eigenspectrum to boundary conditions with the emergence of the non-Hermitian skin effect (NHSE). A NHSE originates from the point-gap topology of complex eigenspectrum, where an extensive number of eigenstates are anomalously localized at the boundary driven by nonreciprocal dissipation. Two different approaches to create localization are disorder and flat-band spectrum, and their interplay can lead to the anomalous inverse Anderson localization, where the Bernoulli anti-symmetric disorder induces mobility in a full-flat band system in the presence of Aharonov–Bohm (AB) Cage. In this work, we study the localization–delocalization transitions due to the interplay of the point-gap topology, flat band and correlated disorder in the one-dimensional rhombic lattice, where both its Hermitian and non-Hermitian structures show AB cage in the presence of magnetic flux. Although it remains the coexistence of localization and delocalization for the Hermitian rhombic lattice in the presence of the random anti-symmetric disorder, it surprisingly becomes complete delocalization, accompanied by the emergence of NHSE. To further study the effects from the Bernoulli anti-symmetric disorder, we found the similar NHSE due to the interplay of the point-gap topology, correlated disorder and flat bands. Our anomalous localization–delocalization property can be experimentally tested in the classical physical platform, such as electrical circuit.

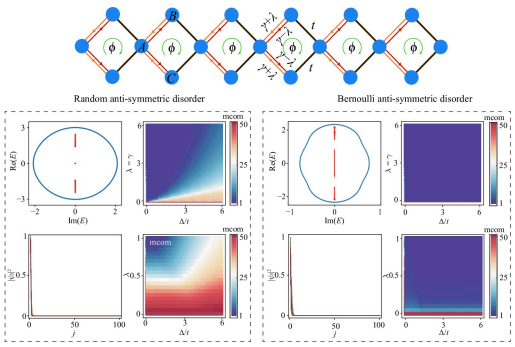

Keywords non-Hermitian skin effects, disorder, flat band, localization–delocalization transition

1 Introduction

Recent years have witnessed tremendous advancements in exploring the physics of non-Hermitian Hamiltonian in open systems due to their unique physical features without Hermitian counterparts [1–61]. The non-Hermitian Hamiltonian can be experimentally realized in classical systems, such as phononic lattice [62], optical structures [63, 64] and electrical circuits [65, 66], and open quantum systems in ultracold atoms [51, 67]. Recent advances in non-Hermitian studies have shown many intriguing potential applications of the non-Hermitian systems in photonics [16, 68, 69] and electrical circuits [70, 71]. One of striking physical features in non-Hermitian systems is the extreme sensitivity of the eigenspectrum to boundary conditions with the emergence of the non-

Higher Education Press

https://doi.org/10.1007/s11467-024-1412-9

Hermitian skin effect (NHSE) [7–9, 17–19, 35–40], where a large number of bulk modes collapse into localized boundary modes in the open boundaries. The NHSE originates from the point-gap topology of the complex eigenspectrum, and has been shown to be responsible for many intriguing physical phenomena in non-Hermitian systems, such as the breakdown of conventional Bloch band theory [7–9] and nonunitary scaling of non-Hermitian localization [72].

In contrast to the boundary localization of bulk modes caused by NHSE, the disorder can induce Anderson localization of bulk modes along the lattice [73, 74]. Recent studies have shown that the introduction of disorder into non-Hermitian lattices with NHSE can lead to many unconventional phenomena [72, 75–94], such as Anderson delocalization [75, 78], nonunitary scaling rule of non-Hermitian localization [75] and reentrant NHSE [93]. In addition to the disorder, flat bands can also lead to the localization of bulk modes along the lattice due to the destructive interference among different propagation paths [95, 96], providing another mechanism to confine waves. A paradigmatic example of the flat-band localization is the Aharonov–Bohm (AB) caging, which provides the perfectly localized compact modes with all the bands being flat in, e.g., the one-dimensional (1D) rhombic lattice subjected to an artificial gauge field [97–103]. Note that the interference among different propagation paths and AB caging have been studied in higher dimension [104–108]. However, owing to the diverging effective mass in a flat band, the system becomes very sensitive to the disorder [109, 110]. Remarkably, it has been shown that the Bernoulli anti-symmetric disorder induces a localization–delocalization transition in the 1D rhombic lattice [99, 102, 103]. This striking effect is dubbed the inverse Anderson transition from an insulating to a metallic phase, where the disorder removes geometric localization and restores transport in a lattice with all bands flat.

The interplay of non-Hermiticity and flat band has recently received the extensive attentions [111–117]. Its effects on the flat-band localization in the 1D rhombic lattice have been also reported [118–123]. A natural question to ask is how the interplay of flat band, disorder and point-gap topology determines the localization–delocalization properties in the 1D rhombic lattice. In this work, we consider a 1D rhombic lattice subjected to the nonreciprocal hopping and magnetic flux, where we introduce two kinds of the correlated disorders, i.e., the random anti-symmetric disorder and the Bernoulli anti-symmetric disorder. In the Hermitian case, the Bernoulli anti-symmetric disorder induces the inverse Anderson localization, while it leads to the NHSE in the presence of nonreciprocal hopping. Mostly interesting, the random anti-symmetric disorder causes the coexistence of localization and delocalization in the Hermitian rhombic lattice subjected to the magnetic flux, however, it induces the delocalization and the emergence of NHSE in the presence of the nonreciprocal hopping.

The article is organized as follows. In Section 2, we build the non-Hermitian model in the rhombic lattice, and study the flat-localization for the clean system in the presence of magnetic flux. In Section 3, we study the effects of random anti-symmetric disorder on the localization and delocalization property in the nonreciprocal model. In Section 4, we discuss the effects of Bernoulli anti-symmetric disorder. In Section 5, we describe the experimental proposal for testing our theoretical results using electrical circuits. In Section 6, we conclude the article.

2 Model of non-Hermitian rhombic lattice

We consider a 1D rhombic lattice consisting of three coupled sublattices, indicated by A, B and C in Fig. 1(a). In such a lattice, the asymmetric fermionic hopping within each unit cell is introduced, and a magnetic flux with $U(1)$ Abelian gauge fields is applied to each plaquette. In the presence of disordered onsite potential, the system's Hamiltonian is written as

$$\begin{aligned}\mathcal{H}_0 = & -t\sum_j\left(a_{j+1}^\dagger b_j \mathrm{e}^{\mathrm{i}\phi} + a_{j+1}^\dagger c_j + \mathrm{H.c.}\right)\\ & -(\gamma+\lambda)\sum_j(a_j^\dagger b_j + a_j^\dagger c_j)\\ & -(\gamma-\lambda)\sum_j(b_j^\dagger a_j + c_j^\dagger a_j)\\ & +\sum_{j,\alpha}\Delta_j^{(\alpha)} n_{\alpha,j},\end{aligned} \tag{1}$$

where a_j, b_j and c_j is the annihilation operator at sublattices A, B and C at the jth unit cell, respectively, $\Delta_j^{(\alpha)}$ $(\alpha = A, B, C)$ is the on-site disorder in sublattice α at the jth unit cell, $n_{\alpha,j} = \alpha_j^\dagger \alpha_j$ $(\alpha = a, b, c)$ denotes a density operator, $\gamma \pm \lambda$ represents the intracell asymmetric hopping strengths, and t is the intercell symmetric hopping strength. In the rhombic lattice, a single Peierls phase factor ϕ is used to represent the magnetic flux in each plaquette.

In the absence of disorder in the system, i.e., $\Delta_j^{(\alpha)} = 0$, we plot the complex eigenenergies for $\phi = 0$, as shown in Figs. 1(b1–b3). There exist one flat band and two dispersive bands [see Figs. 1(b1, b2)]. The eigenenergies with periodic boundary conditions (PBCs) form a point gap in the complex plane, and the eigenenergies with open boundary conditions (OBCs) lies inside the loop [see Fig. 1(b3)]. A point gap usually indicates a non-Hermitian skin effect for eigenstates [39]. Figure 1(b4) shows the probability density distribution $|\psi_j|^2$, with $|\psi_j|^2 = |\psi_{j,A}|^2 + |\psi_{j,B}|^2 + |\psi_{j,C}|^2$, for $|E| \neq 0$, under OBC,

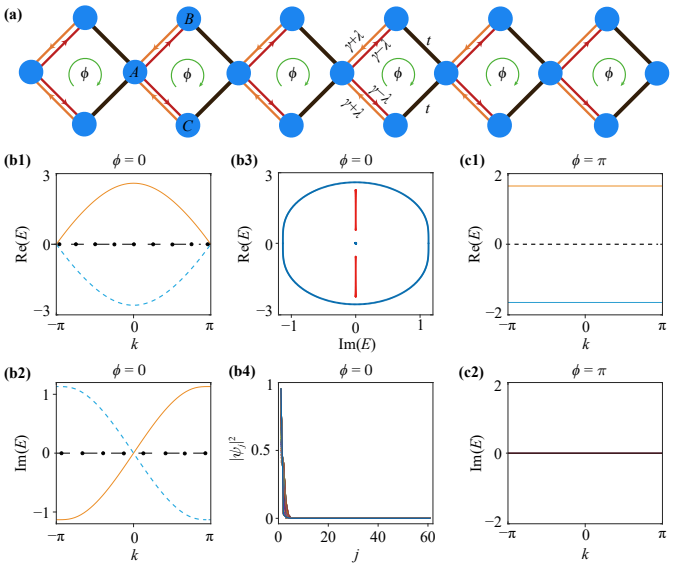

Fig. 1 **(a)** Tight-binding representation of an asymmetric rhombic chain enclosed by a ϕ magnetic flux in each plaquette. Each unit cell contains three sublattices indicated by A, B and C. $\gamma \pm \lambda$ denote the asymmetric hopping strengths (red and yellow lines with arrows), and t is the symmetric hopping strength (black line). Real part **(b1)** and imaginary part **(b2)** of single-particle eigenspectrum for $\phi = 0$. **(b3)** $\mathrm{Re}(E)$ vs. $\mathrm{Im}(E)$ of eigenenergies in complex plane with PBC (blue dots) and OBC (red dots) for $\phi = 0$. **(b4)** Probability density distributions $|\psi_j|^2$ (summed over each unit cell) of eigenstates for their eigenenergies inside point gaps with $|E| \neq 0$ under OBC for $\phi = 0$, where $|\psi_j|^2 = |\psi_{j,A}|^2 + |\psi_{j,B}|^2 + |\psi_{j,C}|^2$. Real part **(c1)** and imaginary part **(c2)** of single-particle eigenspectrum for $\phi = \pi$, and its bands are perfect flat, leading to mode localization. The other parameters are $\gamma/t = 1$ and $\lambda/t = 0.8$.

where all modes with non-zero eigenenergies are localized at left boundaries. While zero-energy eigenstates are localized along the lattice due to the flat-band effect [see Figs. 1(b1, b2), the non-Hermitian skin modes can be characterized by the non-zero spectral winding number, defined as [8, 39]

$$\mathcal{W}(E_r) = \frac{1}{2\pi \mathrm{i}} \int_0^{2\pi} \mathrm{d}k \partial_k \log \det[\mathcal{H}_0(k) - E_r], \tag{2}$$

where E_r is a chosen complex value as a reference energy, and $\mathcal{H}_0(k)$ is momentum-space Hamiltonian with

$$\begin{aligned} \mathcal{H}_0(k) = & -\sum_k t \left[\mathrm{e}^{-\mathrm{i}(k-\phi)} a_k^\dagger b_k + \mathrm{e}^{-\mathrm{i}k} a_k^\dagger c_k + \mathrm{H.c.} \right] \\ & - (\gamma + \lambda) \sum_k \left(a_k^\dagger b_k + a_k^\dagger c_k \right) \\ & - (\gamma - \lambda) \sum_k \left(b_k^\dagger a_k + c_k^\dagger a_k \right). \end{aligned} \tag{3}$$

For $\phi = \pi$, Figs. 1(c1, c2) show three flat bands with perfectly compact localized states, the so-called Aharonov–Bohm cage [100–102, 104] in the non-Hermitian system. In spite of nonreciprocal hopping, the destructive interference effect among different propagation paths greatly suppresses the non-Hermitian skin effect for $\phi = \pi$.

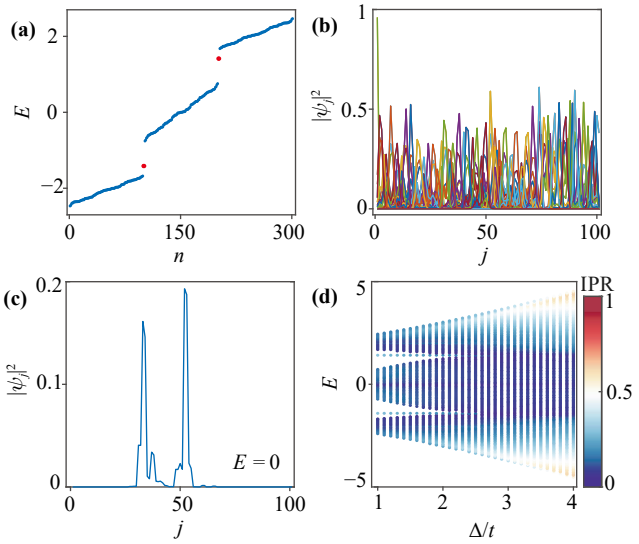

Fig. 2 **(a)** Eigenenergies and **(b)** probability density distributions $|\psi_j|^2$ (summed over each unit cell) of eigenstates of the Hermitian rhombic lattice, subjected to the random anti-symmetric disorder, under OBCs for $\Delta/t = 1$. The red dots indicate the topological boundary states. **(c)** $|\psi_j|^2$ for $E = 0$ with $\Delta/t = 1$. **(d)** IPR vs. Δ. The other parameters for Hermitian conditions are $\phi = \pi$, $\gamma/t = 1$ and $\lambda/t = 0$.

3 Effects of random anti-symmetric disorder

We now consider effects of the interplay of the nonreciprocal hopping and disorder on the mode localization and skin effects. We study two types of disorder realizations: (i) random anti-symmetric disorder, i.e., $\Delta_j^{(B)} = -\Delta_j^{(C)} = \Delta_j$ with Δ_j sampled uniformly in the range $[-\Delta/2, \Delta/2]$, and (ii) correlated binary (Bernoulli) anti-symmetric disorder $\Delta_j^{(B)} = -\Delta_j^{(C)} = \Delta_j$, where Δ_j takes two values $\pm\Delta$ with the same probability [124]. Unless specified otherwise, we assume $\phi = \pi$, and $\Delta_j^{(A)} = 0$.

The strong random anti-symmetric disorder breaks the flatness of bulk bands, and leads to a part of Anderson localization of eigenstates in the Hermitian rhombic lattice, as shown in Figs. 2(a, b). While, for the eigenenergies around zero, the eigenstates are extended [see Fig. 2(c)]. This indicates that disorder-induced transport in the photonic cage system is possible. The 1D rhombic lattice supports topologically-protected in-gap states [see red dots in Fig. 2(a)], which has been experimentally observed [101].

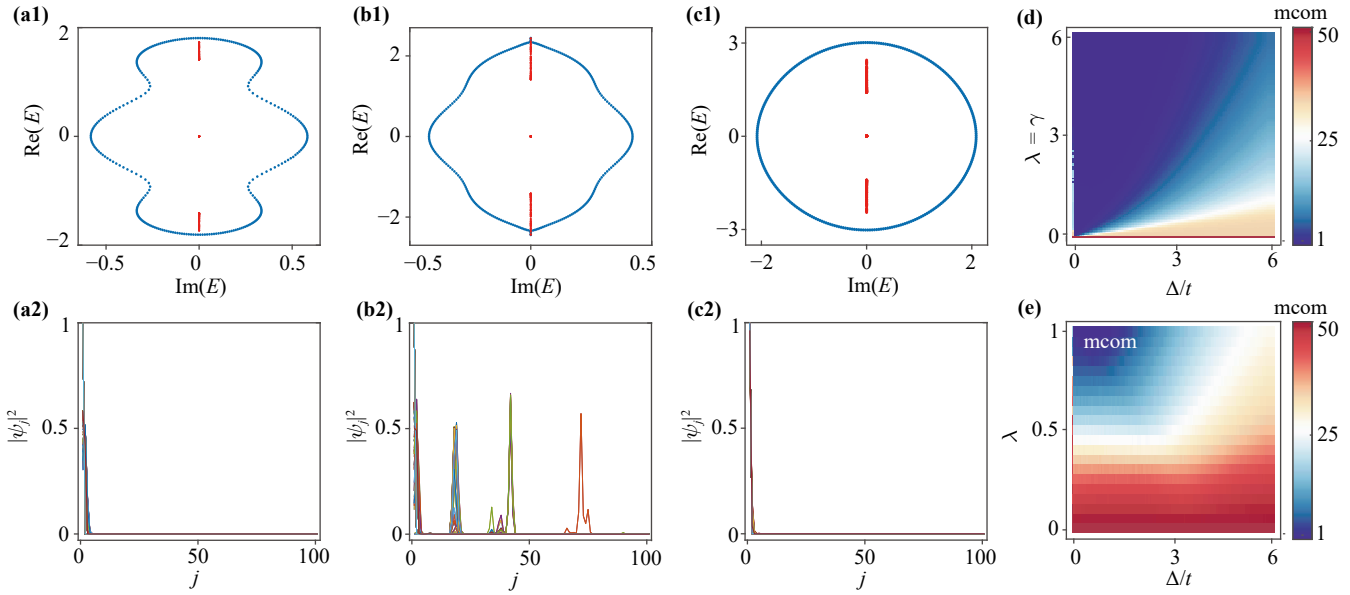

Fig. 3 The localization and delocalization of the non-Hermitian rhombic lattice subjected to random anti-symmetric disorder $\Delta_j^{(B)} = -\Delta_j^{(C)} = \Delta_j$ ($\Delta_j \in [-\Delta/2, \Delta/2]$) for $\phi = \pi$. Complex eigenenergies under both OBCs (blue dots) and PBCs (red dots) **(a1)** for $\Delta/t = 1$ and $\lambda/t = \gamma/t = 1$, **(b1)** for $\Delta/t = 2$ and $\lambda/t = \gamma/t = 1$, and **(c1)** for $\Delta/t = 2$ and $\lambda/t = \gamma/t = 5$. The corresponding probability density distributions $|\psi_j|^2$ (summed over each unit cell) of eigenstates are shown in **(a2, b2, c2)**. **(d)** mcom as functions of λ and Δ with $\lambda = \gamma$. **(e)** mcom as functions of λ and Δ with $\gamma/t = 1$. The mcom is averaged over 2000 disorder realization with $N = 100$.

To characterize the delocalization and localization induced by the random anti-symmetric disorder in a wide range of disorder strength Δ, we calculate the inverse participation ratio (IPR) of each normalized right eigenstate $\psi_n = (\psi_n^{(a)}, \psi_n^{(b)}, \psi_n^{(c)})^{\mathrm{T}}$. The IPR is defined as

$$\mathrm{IPR}_n = \sum_j \left(|\psi_n^{(a)}(j)|^4 + |\psi_n^{(b)}(j)|^4 + |\psi_n^{(c)}(j)|^4 \right), \quad (4)$$

where the sums run over length L of the rhombic chain, and $\sum_j \left(|\psi_n^{(A)}(j)|^2 + |\psi_n^{(B)}(j)|^2 + |\psi_n^{(C)}(j)|^2 \right) = 1$. If the nth eigenstate ψ_n is extended, $\mathrm{IPR}_n \simeq 1/(3L)$ and drops to zero for an infinite system. On the contrary, for the localized eigenstate ψ_n, IPR_n keeps finite, and $\mathrm{IPR}_n \simeq 1$ for the perfect localization. Figure 2(d) plots the eigenenergy-resolved IPR as a function of disorder strength Δ. The random anti-symmetric disorder leads to the coexistence of localized and delocalized eigenstates in the Hermitian rhombic lattice.

We now proceed to study the effects of the random anti-symmetric disorder on the localization–delocalization properties of the rhombic lattice in the presence of nonreciprocal hopping. Figures 3(a1, a2), (b1, b2) and (c1, c2) plot the complex eigenenergies and the corresponding probability density distributions $|\psi_j|^2$ (summed over each unit cell) of eigenstates for different disorder strength Δ and unidirectional hopping strength $\lambda = \gamma$, respectively. In Figs. 3(a1, a2), using the same disorder strength as the one in Figs. 2(a, b), the nonreciprocal hopping leads to the formation of the point gap under PBCs [see blue dots in Fig. 3(a1)], enclosing the eigenenergies under OBCs [see red dots in Fig. 3(a1)]. The point gap usually indicates the emergence of NHSE, where all the bulk modes are localized at the boundaries under OBCs [see Fig. 3(a2)]. The result shows that, although the random anti-symmetric disorder causes the coexistence of localization and delocalization in the Hermitian lattice, the nonreciprocal hopping leads to the complete delocalization, accompanied by the NHSE. Therefore, the interplay of the flat band, disorder and point gap causes an unconventional localization–delocalization property in the rhombic lattice. Further increase of the disorder strength Δ again leads to a part of localization and delocalization, where the skin modes and localized bulk states coexist [see Figs. 3(b1, b2)]. While, the non-Hermitian skin effect reappears for the larger unidirectional hopping strength $\lambda = \gamma$, as shown in Figs. 3(c1, c2). These indicate that the interplay of random anti-symmetric disorder and nonreciprocal hopping can not only breaks the flatness of bulk bands, but also leads to complete delocalization, accompanied by the reentrant NHSE.

To further explore the effects of asymmetrical hopping and disorder strength on the NHSE, we calculate the average eigenstate localization in the form of the mean center of mass (mcom) of the amplitude squared of all eigenvectors ψ_n, averaged over the disorder realization [125], i.e.,

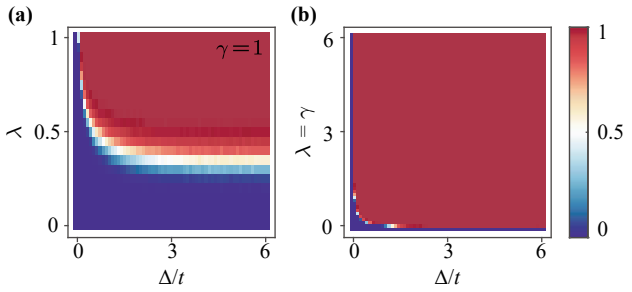

Fig. 4 **(a)** Winding number w as functions of λ and Δ with $\gamma/t = 1$ for the non-Hermitian rhombic lattice subjected to random anti-symmetric disorder. **(b)** Winding number w as functions of λ and Δ with $\lambda = \gamma = 1$ for the non-Hermitian rhombic lattice subjected to random anti-symmetric disorder. The results are averaged over 2000 disorder realizations with $N = 200$.

$$\text{mcom} = \frac{\sum_{j=1}^{N} j \langle \mathcal{A}(j) \rangle_V}{\sum_{j=1}^{N} \langle \mathcal{A}(j) \rangle_V}, \tag{5}$$

with

$$\langle \mathcal{A}(j) \rangle_V = \left\langle \frac{1}{N} \sum_{n=1}^{N} \left(|\psi_n^{(a)}(j)|^2 + |\psi_n^{(b)}(j)|^2 + |\psi_n^{(c)}(j)|^2 \right) \right\rangle_V, \tag{6}$$

where, $\langle \cdot \rangle_V$ indicates disorder averaging, and N is the number of unit cells. The mcom determines the the degree of the mode localization. When mcom is close to be one or N, it indicates the most of eigenstates are localized at the boundaries with the emergence of non-Hermitian skin effect. Otherwise, it indicates the appearance of the delocalized eigenstates.

Figure 3(d) plots the mcom as functions of λ and Δ with $\lambda = \gamma$. When the asymmetrical hopping strength $\lambda = \gamma$ is fixed, the increasing disorder strength Δ leads to the state localization. While, as the $\lambda = \gamma$ rises, the localized states become skin modes, i.e., the emergence of NHSE induced by random anti-symmetric disorder. Moreover, the appearance of NHSE requires a strong asymmetric hopping for the fixed values of γ and Δ, as shown in Fig. 3(e), where we plot the mcom as functions of λ and Δ with $\gamma/t = 1$.

To characterize the topology of non-Hermitian skin effects, we calculate the real-space winding number, which is defined as [85]

$$w(E_b) = \frac{1}{L'} \text{Tr}' \left(\hat{Q}^\dagger [\hat{Q}, \hat{X}] \right), \tag{7}$$

where $\hat{Q}$ is positive-definite Hermitian matrix, which is obtained by the polar decomposition $(\mathcal{H} - E_b) = \hat{Q}\hat{P}$, with unitary matrix $\hat{P}$. $\hat{Q}$ and $\hat{P}$ are related to singular value decomposition $(\mathcal{H}_0 - E_b) = \hat{M}\hat{S}\hat{N}^\dagger$, with $\hat{Q} = \hat{M}\hat{N}^\dagger$ and $\hat{P} = \hat{N}\hat{S}\hat{N}^\dagger$. $\hat{X}$ is the coordinate operator, with $X_{jj',ss'} = j\delta_{j,j'}\delta_{s,s'}(s = a, b)$, and Tr′ denotes the trace over the middle interval with length L', where the whole chain is cut off from both ends. This definition of winding number avoids the effects from the system's boundary.

Figure 4(a) plots the winding number w as functions of λ and Δ with $\gamma/t = 1$ for the non-Hermitian rhombic lattice subjected to the random anti-symmetric disorder. The result shows that the emergence of non-Hermitian effects is strongly determined by the asymmetric strength γ. While, for the perfect unidirectional hopping with $\lambda = \gamma$, even though the disorder is very strong, there exists skin modes [see Fig. 4(b)]. These skin modes are coexistence with the localized modes for the regime with the large mcom [see Figs. 3(b1, b2, d)].

Although the random anti-symmetric disorder leads to the delocalization in the nonreciprocal rhombic lattice subjected to the π gauge field, the random symmetric disorder with $\Delta_j^{(B)} = \Delta_j^{(C)} = \Delta_j$ $(\Delta_j \in [-\Delta/2, \Delta/2])$ leads to the Anderson localization, as shown in Figs. 5(a, b), where there doesn't exist a point gap with the absence

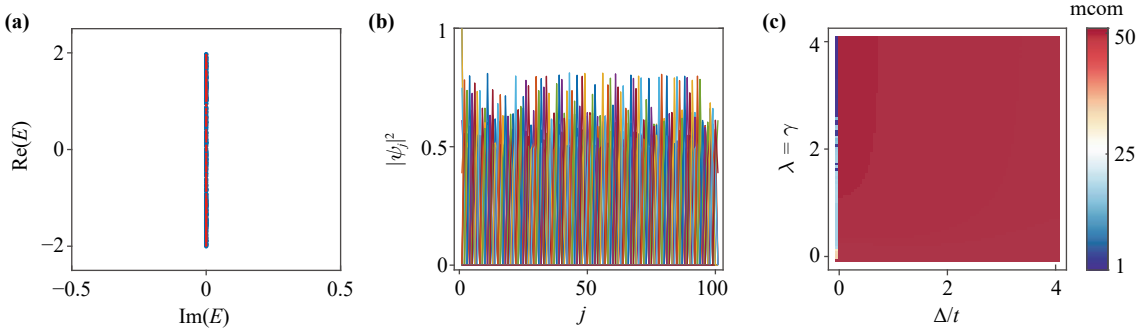

Fig. 5 The localization of the non-Hermitian rhombic lattice subjected to random symmetric disorder $\Delta_j^{(B)} = \Delta_j^{(C)} = \Delta_j$ $(\Delta_j \in [-\Delta/2, \Delta/2])$ for $\phi = \pi$. **(a)** Complex eigenenergies under both OBCs (blue dots) and PBCs (red dots) for $\Delta/t = 1$, and $\lambda/t = \gamma/t = 1$. **(b)** The corresponding probability density distributions $|\psi_j|^2$ (summed over each unit cell) of eigenstates under OBCs. **(c)** mcom as functions of λ and Δ with $\lambda = \gamma$. The mcom is averaged over 2000 disorder realization with $N = 100$.

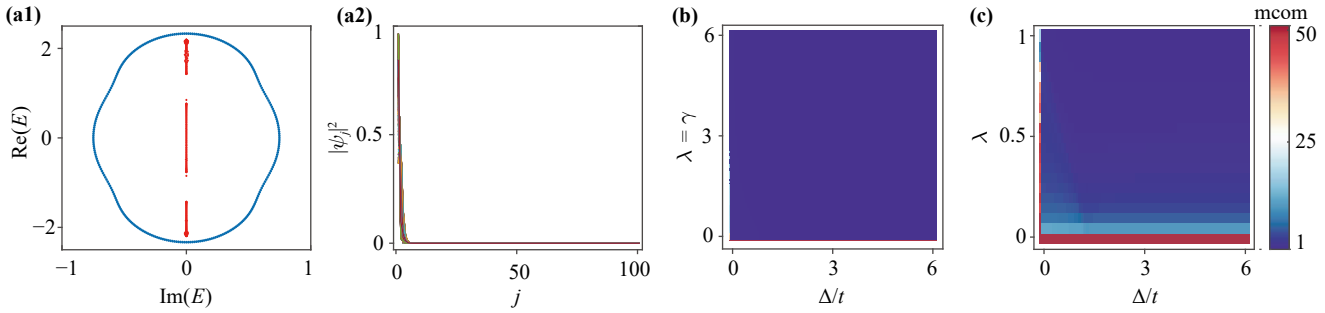

Fig. 6 Localization and delocalization of the non-Hermitian rhombic lattice subjected to Bernoulli anti-symmetric disorder with $\Delta_j^{(B)} = -\Delta_j^{(C)} = \Delta_j$ (Δ_j randomly takes two values of $\pm\Delta$) for $\phi = \pi$. Complex eigenenergies under both OBCs (blue dots) and PBCs (red dots) **(a1)** for $\Delta/t = 1$ and $\lambda/t = \gamma/t = 0.8$. The corresponding probability density distributions $|\psi_j|^2$ (summed over each unit cell) of eigenstates are shown in **(a2)**. **(b)** mcom as functions of λ and Δ with $\lambda = \gamma$. **(c)** mcom as functions of λ and Δ with $\gamma/t = 1$. The mcom is averaged over 2000 disorder realization with $N = 100$.

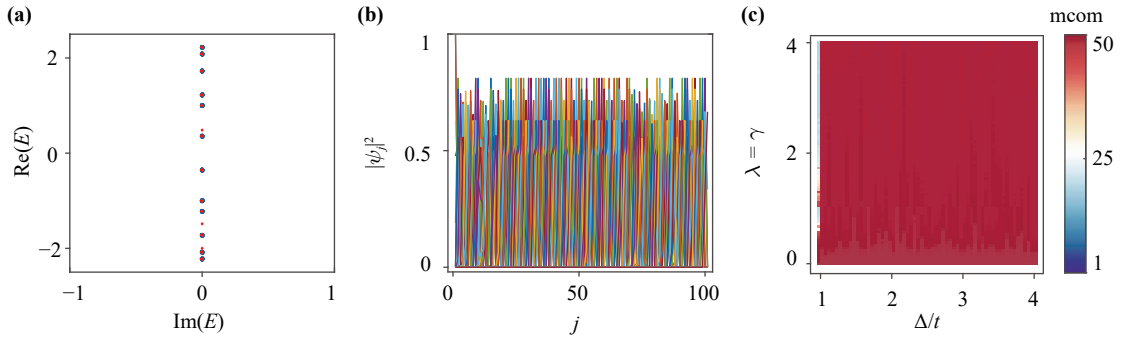

Fig. 7 Localization of the non-Hermitian rhombic lattice subjected to Bernoulli symmetric disorder with $\Delta_j^{(B)} = -\Delta_j^{(C)} = \Delta_j$ (Δ_j randomly takes two values of $\pm\Delta$) for $\phi = \pi$. **(a)** Complex eigenenergies under both OBCs (blue dots) and PBCs (red dots) for $\Delta/t = 1$, and $\lambda/t = \gamma/t = 1$. **(b)** The corresponding probability density distributions $|\psi_j|^2$ (summed over each unit cell) of eigenstates under OBCs f. **(c)** mcom as functions of λ and Δ with $\lambda = \gamma$. The mcom is averaged over 2000 disorder realization with $N = 100$.

of NHSE for $\Delta/t = 1$, and $\lambda/t = \gamma/t = 1$. We calculate the mcom as functions of λ and Δ with $\lambda = \gamma$ in Fig. 5(c). Indeed, when the nonreciprocal rhombic lattice is subjected to the random symmetric disorder, all the states remain localized, and there is no NHSE.

4 Effects of Bernoulli anti-symmetric disorder

The random anti-symmetric disorder cause the coexistence of localized and delocalized states in the Hermitian rhombic lattice subjected to the π flux. while, the interplay of the random anti-symmetric disorder, flat band and point gap leads to the delocalization, accompanied by the reentrant NHSE. In the Hermitian rhombic lattice, it has been shown that the Bernoulli anti-symmetric disorder leads to the inverse Anderson localization due to the interplay of geometric frustration and disorder [124].

We now consider the non-Hermitian rhombic lattice subjected to the Bernoulli anti-symmetric disorder with $\Delta_j^{(B)} = -\Delta_j^{(C)} = \Delta_j$ (Δ_j randomly takes two values of $\pm\Delta$) for $\phi = \pi$. Figure 6(a1) shows the complex eigenenergies of the lattice under both OBCs and PBCs. The point gap (blue dots) enclosing the real eigenvalues (red dots) under OBC indicate the NHSE, as shown in Fig. 6(a2), where all the bulk modes are localized at the left boundary. To explore how the asymmetrical hopping and disorder strength influence the NHSE, we calculate the mcom as functions of $\lambda = \gamma$ and Δ, as shown in Fig. 6(b). In contrast to the case of random anti-symmetric disorder, a small value of the unidirectional hopping strength $\lambda = \gamma$ can induced the NHSE in spite of the disorder strength. Moreover, a small degree of asymmetric hopping can cause the skin modes in spite of the disorder strength [see Fig. 6(c)].

Although the Bernoulli anti-symmetric disorder leads to the delocalization in the nonreciprocal rhombic lattice subjected to the π gauge field, the Bernoulli symmetric disorder with $\Delta_j^{(B)} = \Delta_j^{(C)} = \Delta_j$ (Δ_j randomly takes two values of $\pm\Delta$) leads to the Anderson localization, as shown in Figs. 7(a, b), where there does not exist a

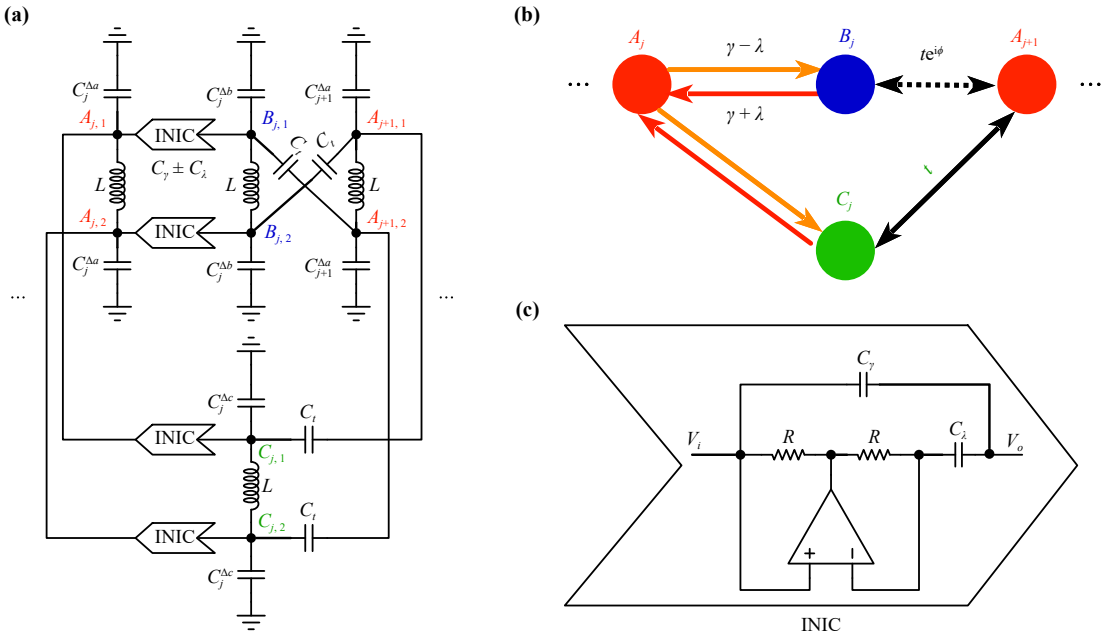

Fig. 8 **(a)** Electrical circuit implementation of the model in Eq. (1), corresponding to the lattice structure in **(b)**. The nonreciprocal hopping between nodes j and $j+1$ is realized by the negative impedance converters through current inversions (INICs). **(c)** Details of INIC.

point gap with the absence of NHSE for $\Delta/t = 1$, and $\lambda/t = \gamma/t = 1$. We calculate the mcom as functions of λ and Δ with $\lambda = \gamma$ in Fig. 7(c). Indeed, when the nonreciprocal rhombic lattice is subjected to the random symmetric disorder, all the states remain localized, and there is no NHSE.

5 Experimental proposal

The localization-delocalization transition induced by the anti-symmetric disorder with the emergence of NHSE can be experimentally observed in the electrical circuits [65, 66]. we design non-Hermitian electrical circuits, corresponding to the model in Eq. (1), as shown in Fig. 8. The nonreciprocal hopping between nodes j and $j+1$ is realized by the negative impedance converters through current inversions (INICs) [126]. The model in Eq. (1) is represented by the circuit Laplacian $J(\omega)$ of the circuit. The Laplacian is defined as the response of the grounded-voltage vector $\boldsymbol{V}$ to the vector $\boldsymbol{I}$ of input current by [127, 128]

$$\boldsymbol{I}(\omega) = J(\omega)\boldsymbol{V}(\omega). \tag{8}$$

In Fig. 8, the negative impedance converter through circuit reads $C_\gamma \pm C_\lambda$, introducing the nonreciprocal intracell hopping in Eq. (1). The grounded capacitors, $C_j^{\Delta a}$, $C_j^{\Delta b}$ and $C_j^{\Delta c}$, represents the on-site disorder of A, B and C sublattices in the jth unit cell. Capacitor C_t is used to represent the symmetrical intercell hopping of the model in Eq. (1). The phase $\phi = \pi$ can be achieved by crossing the adjacent nodes with wires in Fig. 8(a). The inductor L is used to tune the resonant frequency of the circuit. Using Eq. (8), the current of each node within the unit cell can be expressed as

$$\begin{aligned} I_{a,j} = {} & \mathrm{i}\omega\left(C_\gamma + C_\lambda\right)\mathcal{I}_2 V_{b,j} + \mathrm{i}\omega C_t \mathcal{I}_2 V_{c,j-1} \\ & + \mathrm{i}\omega C_t \begin{pmatrix} 0 & 1 \\ 1 & 0 \end{pmatrix} V_{b,j-1} + \mathrm{i}\omega\left(C_\gamma + C_\lambda\right)\mathcal{I}_2 V_{c,j} \\ & + \frac{1}{\mathrm{i}\omega L}\begin{pmatrix} -1 & 1 \\ 1 & -1 \end{pmatrix} V_{a,j} \\ & - \mathrm{i}\omega\left(2C_\gamma + 2C_\lambda + 2C_t + C_j^{\Delta a}\right)\mathcal{I}_2 V_{a,j}, \end{aligned} \tag{9}$$

$$\begin{aligned} I_{b,j} = {} & \mathrm{i}\omega\left(C_\gamma - C_\lambda\right)\mathcal{I}_2 V_{a,j} + \mathrm{i}\omega C_t \begin{pmatrix} 0 & 1 \\ 1 & 0 \end{pmatrix} V_{a,j+1} \\ & + \frac{1}{\mathrm{i}\omega L}\begin{pmatrix} -1 & 1 \\ 1 & -1 \end{pmatrix} V_{b,j} \\ & - \mathrm{i}\omega\left(C_\gamma - C_\lambda + C_t + C_j^{\Delta b}\right)\mathcal{I}_2 V_{b,j}, \end{aligned} \tag{10}$$

$$\begin{aligned} I_{c,j} = {} & \mathrm{i}\omega\left(C_\gamma - C_\lambda\right)\mathcal{I}_2 V_{a,j} + \mathrm{i}\omega C_t \mathcal{I}_2 V_{a,j+1} \\ & + \frac{1}{\mathrm{i}\omega L}\begin{pmatrix} -1 & 1 \\ 1 & -1 \end{pmatrix} V_{c,j} \\ & - \mathrm{i}\omega\left(C_\gamma - C_\lambda + C_t + C_j^{\Delta c}\right)\mathcal{I}_2 V_{c,j}, \end{aligned} \tag{11}$$

where the vectors $I_{\alpha,j} = (I_{\alpha,1,j},\ I_{\alpha,2,j})^{\mathrm{T}}$ $(\alpha = a, b, c)$ and $V_{\alpha,j} = (V_{\alpha,1,j},\ V_{\alpha,2,j})^{\mathrm{T}}$ $(\alpha = a, b, c)$ denote the node currents and voltages of A, B and C sublattices within the jth unit cell, respectively, and $\mathcal{I}_2$ represents the 2×2 identity matrix.

We transform Eqs. (9)–(11) using a unitary matrix

$$U=\frac{1}{\sqrt{2}}\begin{pmatrix}1 & 1\\ 1 & -1\end{pmatrix}, \tag{12}$$

and achieve the transformed current–voltage relationship:

$$\begin{aligned}\bar{I}_{a,j}=&\,\mathrm{i}\omega\left(C_\gamma+C_\lambda\right)\mathcal{I}_2\bar{V}_{b,j}+\mathrm{i}\omega C_t\mathcal{I}_2\bar{V}_{c,j-1}\\&+\mathrm{i}\omega C_t\begin{pmatrix}1 & 0\\ 0 & \mathrm{e}^{\mathrm{i}\pi}\end{pmatrix}\bar{V}_{b,j-1}+\mathrm{i}\omega\left(C_\gamma+C_\lambda\right)\mathcal{I}_2\bar{V}_{c,j}\\&+\frac{1}{\mathrm{i}\omega L}\begin{pmatrix}0 & 0\\ 0 & -2\end{pmatrix}\bar{V}_{a,j}\\&-\mathrm{i}\omega\left(2C_\gamma+2C_\lambda+2C_t+C_j^{\Delta a}\right)\mathcal{I}_2\bar{V}_{a,j},\end{aligned} \tag{13}$$

$$\begin{aligned}\bar{I}_{b,j}=&\,\mathrm{i}\omega\left(C_\gamma-C_\lambda\right)\mathcal{I}_2\bar{V}_{a,j}+\mathrm{i}\omega C_t\begin{pmatrix}1 & 0\\ 0 & \mathrm{e}^{\mathrm{i}\pi}\end{pmatrix}\bar{V}_{a,j+1}\\&+\frac{1}{\mathrm{i}\omega L}\begin{pmatrix}0 & 0\\ 0 & -2\end{pmatrix}\bar{V}_{b,j}\\&-\mathrm{i}\omega\left(C_\gamma-C_\lambda+C_t+C_j^{\Delta b}\right)\mathcal{I}_2\bar{V}_{b,j},\end{aligned} \tag{14}$$

$$\begin{aligned}\bar{I}_{c,j}=&\,\mathrm{i}\omega\left(C_\gamma-C_\lambda\right)\mathcal{I}_2\bar{V}_{a,j}+\mathrm{i}\omega C_t\mathcal{I}_2\bar{V}_{a,j+1}\\&+\frac{1}{\mathrm{i}\omega L}\begin{pmatrix}0 & 0\\ 0 & -2\end{pmatrix}\bar{V}_{c,j}\\&-\mathrm{i}\omega\left(C_\gamma-C_\lambda+C_t+C_j^{\Delta c}\right)\mathcal{I}_2\bar{V}_{c,j}.\end{aligned} \tag{15}$$

As shown in Eqs. (13)–(15), after the unitary transformation, the current–voltage equations at second node is decoupled with ones at first node, and the phase $\mathrm{e}^{\mathrm{i}\pi}$ of the intercell hopping appears in the second node of the circuit. Therefore, we only need to consider the circuit Laplacian at second node. We rewrite the current–voltage equations for the second nodes as

$$\begin{aligned}\bar{I}_{a,2,j}=&\,\mathrm{i}\omega\left(C_\gamma+C_\lambda\right)\bar{V}_{b,2,j}+\mathrm{i}\omega C_t\bar{V}_{c,2,j-1}\\&+\mathrm{i}\omega C_t\mathrm{e}^{\mathrm{i}\pi}\bar{V}_{b,2,j-1}+\mathrm{i}\omega\left(C_\gamma+C_\lambda\right)\bar{V}_{c,2,j}\\&-\frac{2}{\mathrm{i}\omega L}\bar{V}_{a,2,j}-\mathrm{i}\omega\left(2C_\gamma+2C_\lambda+2C_t+C_j^{\Delta a}\right)\bar{V}_{a,2,j},\end{aligned} \tag{16}$$

$$\begin{aligned}\bar{I}_{b,2,j}=&\,\mathrm{i}\omega\left(C_\gamma-C_\lambda\right)\bar{V}_{a,2,j}+\mathrm{i}\omega C_t\mathrm{e}^{\mathrm{i}\pi}\bar{V}_{a,2,j+1}\\&-\frac{2}{\mathrm{i}\omega L}\bar{V}_{b,2,j}-\mathrm{i}\omega\left(C_\gamma-C_\lambda+C_t+C_j^{\Delta b}\right)\bar{V}_{b,2,j},\end{aligned} \tag{17}$$

$$\begin{aligned}\bar{I}_{c,2,j}=&\,\mathrm{i}\omega\left(C_\gamma-C_\lambda\right)V^*_{a,2,j}+\mathrm{i}\omega C_t\bar{V}_{a,2,j+1}\\&-\frac{2}{\mathrm{i}\omega L}\bar{V}_{c,2,j}-\mathrm{i}\omega\left(C_\gamma-C_\lambda+C_t+C_j^{\Delta c}\right)\bar{V}_{c,2,j},\end{aligned} \tag{18}$$

where $\bar{I}_{\alpha,2,j}\ (\alpha=a,b,c)$ and $\bar{V}_{\alpha,2,j}\ (\alpha=a,b,c)$ denote the current and voltage of the second node within each sublattice in circuit, respectively. Therefore, we achieve the targeted circuit Laplacian $J(\omega)$ to simulate the model in Eq. (1) as

$$\mathcal{J}=\mathrm{i}\omega\begin{pmatrix}\eta_{\Delta a} & C_\gamma+C_\lambda & C_\gamma+C_\lambda & \cdots & 0 & 0 & 0\\ C_\gamma-C_\lambda & \eta_{\Delta b} & 0 & \cdots & 0 & 0 & 0\\ C_\gamma-C_\lambda & 0 & \eta_{\Delta c} & \cdots & 0 & 0 & 0\\ \vdots & \vdots & \vdots & \ddots & \vdots & \vdots & \vdots\\ 0 & 0 & 0 & \cdots & \eta_{\Delta a} & C_\gamma+C_\lambda & C_\gamma+C_\lambda\\ 0 & 0 & 0 & \cdots & C_\gamma-C_\lambda & \eta_{\Delta b} & 0\\ 0 & 0 & 0 & \cdots & C_\gamma-C_\lambda & 0 & \eta_{\Delta c}\end{pmatrix}, \tag{19}$$

where $\eta_\alpha=\frac{2}{\omega^2L}-\left(M+C_j^\alpha\right)\ (\alpha=\Delta a,\Delta b,\Delta c)$ with $M=2C_\gamma+2C_\lambda+2C_t$, $N=C_\gamma-C_\lambda+C_t$.

6 Conclusion

In this work, we study how the nonreciprocal hopping determines the localization and delocalization properties in the 1D rhombic lattice subjected to the magnetic flux and correlated disorder. When the Bernoulli anti-symmetric disorder is introduced into the non-Hermitian rhombic lattice, it leads to the boundary localization of the bulk modes in spite of the disorder strength. To be interesting, a small degree of asymmetric hopping can cause the NHSE. When the random anti-symmetric disorder is introduced into the non-Hermitian rhombic lattice, it leads to the anomalous delocalization, accompanied by the NHSE, while the random anti-symmetric disorder causes the coexistence of localization and delocalization in the Hermitian rhombic lattice. Moreover, the localization–delocalization transition strongly depends on the disorder strength and asymmetric hopping strength. The experimental setup for observing the effects of the point-gap, flat band correlated disorder is proposed in electrical circuits.

Declarations The authors declare that they have no competing interests and there are no conflicts.

Acknowledgements T.L. acknowledges the support from the Fundamental Research Funds for the Central Universities (Grant No. 2023ZYGXZR020), the Introduced Innovative Team Project of Guangdong Pearl River Talents Program (Grant No. 2021ZT09Z109), and the Startup Grant of South China University of Technology (Grant No. 20210012).

References

1. V. V. Konotop, J. Yang, and D. A. Zezyulin, Nonlinear waves in PT-symmetric systems, *Rev. Mod. Phys.* 88(3), 035002 (2016)
2. T. E. Lee, Anomalous edge state in a non-Hermitian lattice, *Phys. Rev. Lett.* 116(13), 133903 (2016)
3. D. Leykam, K. Y. Bliokh, C. Huang, Y. D. Chong, and F. Nori, Edge modes, degeneracies, and topological numbers in non-Hermitian systems, *Phys. Rev. Lett.* 118(4), 040401 (2017)
4. Y. Xu, S. T. Wang, and L. M. Duan, Weyl exceptional rings in a three-dimensional dissipative cold atomic gas, *Phys. Rev. Lett.* 118(4), 045701 (2017)
5. Z. Gong, Y. Ashida, K. Kawabata, K. Takasan, S. Higashikawa, and M. Ueda, Topological phases of non-Hermitian systems, *Phys. Rev. X* 8(3), 031079 (2018)
6. R. El-Ganainy, K. G. Makris, M. Khajavikhan, Z. H. Musslimani, S. Rotter, and D. N. Christodoulides, Non-Hermitian physics and PT symmetry, *Nat. Phys.* 14(1), 11 (2018)
7. S. Yao and Z. Wang, Edge states and topological invariants of non-Hermitian systems, *Phys. Rev. Lett.* 121(8), 086803 (2018)
8. K. Zhang, Z. Yang, and C. Fang, Correspondence between winding numbers and skin modes in non-Hermitian systems, *Phys. Rev. Lett.* 125(12), 126402 (2020)
9. K. Yokomizo and S. Murakami, Non-Bloch band theory of non-Hermitian systems, *Phys. Rev. Lett.* 123(6), 066404 (2019)
10. T. Gao, E. Estrecho, K. Y. Bliokh, T. C. H. Liew, M. D. Fraser, S. Brodbeck, M. Kamp, C. Schneider, S. Höfling, Y. Yamamoto, F. Nori, Y. S. Kivshar, A. G. Truscott, R. G. Dall, and E. A. Ostrovskaya, Observation of non-Hermitian degeneracies in a chaotic exciton–polariton billiard, *Nature* 526(7574), 554 (2015)
11. C. Y. Ju, A. Miranowicz, G. Y. Chen, and F. Nori, Non-Hermitian Hamiltonians and no–go theorems in quantum information, *Phys. Rev. A* 100(6), 062118 (2019)
12. F. Minganti, A. Miranowicz, R. W. Chhajlany, and F. Nori, Quantum exceptional points of non-Hermitian Hamiltonians and Liouvillians: The effects of quantum jumps, *Phys. Rev. A* 100(6), 062131 (2019)
13. B. Peng, Ş. K. Özdemir, F. Lei, F. Monifi, M. Gianfreda, G. L. Long, S. Fan, F. Nori, C. M. Bender, and L. Yang, Parity–time-symmetric whispering-gallery microcavities, *Nat. Phys.* 10(5), 394 (2014)
14. B. Peng, Ş. K. Özdemir, S. Rotter, H. Yilmaz, M. Liertzer, F. Monifi, C. M. Bender, F. Nori, and L. Yang, Loss-induced suppression and revival of lasing, *Science* 346(6207), 328 (2014)
15. Z. P. Liu, J. Zhang, Ş. K. Özdemir, B. Peng, H. Jing, X. Y. Lü, C. W. Li, L. Yang, F. Nori, and Y. Liu, Metrology with PT-symmetric cavities: Enhanced sensitivity near the PT-phase transition, *Phys. Rev. Lett.* 117(11), 110802 (2016)
16. Ş. K. Özdemir, S. Rotter, F. Nori, and L. Yang, Parity–time symmetry and exceptional points in photonics, *Nat. Mater.* 18(8), 783 (2019)
17. S. Yao, F. Song, and Z. Wang, Non-Hermitian Chern bands, *Phys. Rev. Lett.* 121(13), 136802 (2018)
18. F. K. Kunst, E. Edvardsson, J. C. Budich, and E. J. Bergholtz, Biorthogonal bulk-boundary correspondence in non-Hermitian systems, *Phys. Rev. Lett.* 121(2), 026808 (2018)
19. T. Liu, Y. R. Zhang, Q. Ai, Z. Gong, K. Kawabata, M. Ueda, and F. Nori, Second-order topological phases in non-Hermitian systems, *Phys. Rev. Lett.* 122(7), 076801 (2019)
20. K. Y. Bliokh, D. Leykam, M. Lein, and F. Nori, Topological non-Hermitian origin of surface Maxwell waves, *Nat. Commun.* 10(1), 580 (2019)
21. F. Song, S. Yao, and Z. Wang, Non-Hermitian skin effect and chiral damping in open quantum systems, *Phys. Rev. Lett.* 123(17), 170401 (2019)
22. J. Y. Lee, J. Ahn, H. Zhou, and A. Vishwanath, Topological correspondence between Hermitian and non-Hermitian systems: Anomalous dynamics, *Phys. Rev. Lett.* 123(20), 206404 (2019)
23. K. Kawabata, T. Bessho, and M. Sato, Classification of exceptional points and non-Hermitian topological semimetals, *Phys. Rev. Lett.* 123(6), 066405 (2019)
24. C. H. Lee and R. Thomale, Anatomy of skin modes and topology in non-Hermitian systems, *Phys. Rev. B* 99(20), 201103 (2019)
25. A. Fan and S. D. Liang, Complex energy plane and topological invariant in non-Hermitian systems, *Front. Phys.* 17(3), 33501 (2022)
26. G. Sun, J. C. Tang, and S. P. Kou, Biorthogonal quantum criticality in non-Hermitian many-body systems, *Front. Phys.* 17(3), 33502 (2021)
27. Y. P. Wu, G. Q. Zhang, C. X. Zhang, J. Xu, and D. W. Zhang, Interplay of nonreciprocity and nonlinearity on mean-field energy and dynamics of a Bose–Einstein condensate in a double-well potential, *Front. Phys.* 17(4), 42503 (2022)
28. Y. T. Zhang, S. Jiang, Q. Li, and Q. F. Sun, An analytical solution for quantum scattering through a PT-symmetric delta potential, *Front. Phys.* 16(4), 43503 (2021)
29. Z. Y. Ge, Y. R. Zhang, T. Liu, S. W. Li, H. Fan, and F. Nori, Topological band theory for non-Hermitian systems from the Dirac equation, *Phys. Rev. B* 100(5), 054105 (2019)
30. H. Zhou and J. Y. Lee, Periodic table for topological bands with non-Hermitian symmetries, *Phys. Rev. B* 99(23), 235112 (2019)
31. H. Zhao, X. Qiao, T. Wu, B. Midya, S. Longhi, and L. Feng, Non-Hermitian topological light steering, *Science* 365(6458), 1163 (2019)
32. K. Kawabata, K. Shiozaki, M. Ueda, and M. Sato, Symmetry and topology in non-Hermitian physics, *Phys. Rev. X* 9(4), 041015 (2019)
33. D. S. Borgnia, A. J. Kruchkov, and R. J. Slager, Non-Hermitian boundary modes and topology, *Phys. Rev. Lett.* 124(5), 056802 (2020)
34. T. Liu, J. J. He, T. Yoshida, Z. L. Xiang, and F. Nori, Non-Hermitian topological Mott insulators in one-

dimensional fermionic superlattices, *Phys. Rev. B* 102(23), 235151 (2020)
35. L. Li, C. H. Lee, S. Mu, and J. Gong, Critical non-Hermitian skin effect, *Nat. Commun.* 11(1), 5491 (2020)
36. K. Yokomizo and S. Murakami, Scaling rule for the critical non-Hermitian skin effect, *Phys. Rev. B* 104(16), 165117 (2021)
37. Y. Ashida, Z. Gong, and M. Ueda, Non-Hermitian physics, *Adv. Phys.* 69(3), 249 (2020)
38. K. Kawabata, M. Sato, and K. Shiozaki, Higher-order non-Hermitian skin effect, *Phys. Rev. B* 102(20), 205118 (2020)
39. N. Okuma, K. Kawabata, K. Shiozaki, and M. Sato, Topological origin of non-Hermitian skin effects, *Phys. Rev. Lett.* 124(8), 086801 (2020)
40. Y. Yi and Z. Yang, Non-Hermitian skin modes induced by on-site dissipations and chiral tunneling effect, *Phys. Rev. Lett.* 125(18), 186802 (2020)
41. T. Liu, J. J. He, Z. Yang, and F. Nori, Higher-order Weyl-exceptional-ring semimetals, *Phys. Rev. Lett.* 127(19), 196801 (2021)
42. L. Li, C. H. Lee, and J. Gong, Impurity induced scale-free localization, *Commun. Phys.* 4(1), 42 (2021)
43. C. Chen, Y. Liu, L. Zhao, X. Hu, and Y. Fu, Asymmetric nonlinear-mode-conversion in an optical waveguide with PT symmetry, *Front. Phys.* 17(5), 52504 (2022)
44. E. J. Bergholtz, J. C. Budich, and F. K. Kunst, Exceptional topology of non-Hermitian systems, *Rev. Mod. Phys.* 93(1), 015005 (2021)
45. Y. Li, C. Liang, C. Wang, C. Lu, and Y. C. Liu, Gain-loss-induced hybrid skin-topological effect, *Phys. Rev. Lett.* 128(22), 223903 (2022)
46. K. Zhang, Z. Yang, and C. Fang, Universal non-Hermitian skin effect in two and higher dimensions, *Nat. Commun.* 13(1), 2496 (2022)
47. K. Li and Y. Xu, Non-Hermitian absorption spectroscopy, *Phys. Rev. Lett.* 129(9), 093001 (2022)
48. Y. Wang, J. Lin, and P. Xu, Transmission-reflection decoupling of non-Hermitian photonic doping epsilon-near- zero media, *Front. Phys.* 19(3), 33206 (2024)
49. J. R. Li, C. Jiang, H. Su, D. Qi, L. L. Zhang, and W. J. Gong, Parity-dependent skin effects and topological properties in the multilayer nonreciprocal Su–Schrieffer –Heeger structures, *Front. Phys.* 19(3), 33204 (2024)
50. Y. Y. Zou, Y. Zhou, L. M. Chen, and P. Ye, Detecting bulk and edge exceptional points in non-Hermitian systems through generalized Petermann factors, *Front. Phys.* 19(2), 23201 (2024)
51. Z. Ren, D. Liu, E. Zhao, C. He, K. K. Pak, J. Li, and G. B. Jo, Chiral control of quantum states in non-Hermitian spin–orbit-coupled fermions, *Nat. Phys.* 18(4), 385 (2022)
52. K. Kawabata, T. Numasawa, and S. Ryu, Entanglement phase transition induced by the non-Hermitian skin effect, *Phys. Rev. X* 13(2), 021007 (2023)
53. R. Lin, T. Tai, L. Li, and C. H. Lee, Topological non-Hermitian skin effect, *Front. Phys.* 18(5), 53605 (2023)
54. K. Zhang, C. Fang, and Z. Yang, Dynamical degeneracy splitting and directional invisibility in non-Hermitian systems, *Phys. Rev. Lett.* 131(3), 036402 (2023)
55. C. A. Li, B. Trauzettel, T. Neupert, and S. B. Zhang, Enhancement of second-order non-Hermitian skin effect by magnetic fields, *Phys. Rev. Lett.* 131(11), 116601 (2023)
56. N. Okuma and M. Sato, Non-Hermitian topological phenomena: A review, *Annu. Rev. Condens. Matter Phys.* 14(1), 83 (2023)
57. Z. F. Cai, T. Liu, and Z. Yang, Non-Hermitian skin effect in periodically-driven dissipative ultracold atoms, arXiv: 2311.06550 (2023)
58. C. Leefmans, A. Dutt, J. Williams, L. Yuan, M. Parto, F. Nori, S. Fan, and A. Marandi, Topological dissipation in a time-multiplexed photonic resonator network, *Nat. Phys.* 18(4), 442 (2022)
59. C. R. Leefmans, M. Parto, J. Williams, G. H. Y. Li, A. Dutt, F. Nori, and A. Marandi, Topological temporally mode-locked laser, *Nat. Phys.*, doi: 10.1038/s41567-024-02420-4 (2024)
60. H. Zhang, Z. Guo, Y. Li, Y. Yang, Y. Chen, and H. Chen, A universal non-Hermitian platform for bound state in the continuum enhanced wireless power transfer, *Front. Phys.* 19(4), 43209 (2024)
61. X. D. Xie, Z. Y. Xue, and D. B. Zhang, Variational quantum algorithms for scanning the complex spectrum of non-Hermitian systems, *Front. Phys.* 19(4), 41202 (2024)
62. Q. Zhou, J. Wu, Z. Pu, J. Lu, X. Huang, W. Deng, M. Ke, and Z. Liu, Observation of geometry-dependent skin effect in non-Hermitian phononic crystals with exceptional points, *Nat. Commun.* 14(1), 4569 (2023)
63. S. Weidemann, M. Kremer, T. Helbig, T. Hofmann, A. Stegmaier, M. Greiter, R. Thomale, and A. Szameit, Topological funneling of light, *Science* 368(6488), 311 (2020)
64. K. Wang, A. Dutt, K. Y. Yang, C. C. Wojcik, J. Vučković, and S. Fan, Generating arbitrary topological windings of a non-Hermitian band, *Science* 371(6535), 1240 (2021)
65. T. Helbig, T. Hofmann, S. Imhof, M. Abdelghany, T. Kiessling, L. W. Molenkamp, C. H. Lee, A. Szameit, M. Greiter, and R. Thomale, Generalized bulk–boundary correspondence in non-Hermitian topolectrical circuits, *Nat. Phys.* 16(7), 747 (2020)
66. D. Zou, T. Chen, W. He, J. Bao, C. H. Lee, H. Sun, and X. Zhang, Observation of hybrid higher-order skin-topological effect in non-Hermitian topolectrical circuits, *Nat. Commun.* 12(1), 7201 (2021)
67. Q. Liang, D. Xie, Z. Dong, H. Li, H. Li, B. Gadway, W. Yi, and B. Yan, Dynamic signatures of non-Hermitian skin effect and topology in ultracold atoms, *Phys. Rev. Lett.* 129(7), 070401 (2022)
68. L. Feng, R. El-Ganainy, and L. Ge, Non-Hermitian photonics based on parity–time symmetry, *Nat. Photonics* 11(12), 752 (2017)
69. R. El-Ganainy, K. G. Makris, M. Khajavikhan, Z. H. Musslimani, S. Rotter, and D. N. Christodoulides, Non-Hermitian physics and PT symmetry, *Nat. Phys.* 14(1), 11 (2018)
70. Y. Wu, L. Kang, and D. H. Werner, Generalized PT symmetry in non-Hermitian wireless power transfer systems, *Phys. Rev. Lett.* 129(20), 200201 (2022)

71. X. Hao, K. Yin, J. Zou, R. Wang, Y. Huang, X. Ma, and T. Dong, Frequency-stable robust wireless power transfer based on high-order pseudo-Hermitian physics, *Phys. Rev. Lett.* 130(7), 077202 (2023)
72. K. Kawabata and S. Ryu, Nonunitary scaling theory of non-Hermitian localization, *Phys. Rev. Lett.* 126(16), 166801 (2021)
73. P. W. Anderson, Absence of diffusion in certain random lattices, *Phys. Rev.* 109(5), 1492 (1958)
74. P. A. Lee and T. V. Ramakrishnan, Disordered electronic systems, *Rev. Mod. Phys.* 57(2), 287 (1985)
75. N. Hatano and D. R. Nelson, Localization transitions in non-Hermitian quantum mechanics, *Phys. Rev. Lett.* 77(3), 570 (1996)
76. N. Hatano and D. R. Nelson, Non-Hermitian delocalization and eigenfunctions, *Phys. Rev. B* 58(13), 8384 (1998)
77. J. Feinberg and A. Zee, Non-Hermitian localization and delocalization, *Phys. Rev. E* 59(6), 6433 (1999)
78. Z. Gong, Y. Ashida, K. Kawabata, K. Takasan, S. Higashikawa, and M. Ueda, Topological phases of non-Hermitian systems, *Phys. Rev. X* 8(3), 031079 (2018)
79. H. Jiang, L. J. Lang, C. Yang, S. L. Zhu, and S. Chen, Interplay of non-Hermitian skin effects and Anderson localization in nonreciprocal quasiperiodic lattices, *Phys. Rev. B* 100(5), 054301 (2019)
80. C. Wang, and X. R. Wang, Level statistics of extended states in random non-Hermitian Hamiltonians, *Phys. Rev. B* 101(16), 165114 (2020)
81. S. Longhi, Topological phase transition in non-Hermitian quasicrystals, *Phys. Rev. Lett.* 122(23), 237601 (2019)
82. A. F. Tzortzakakis, K. G. Makris, and E. N. Economou, Non-Hermitian disorder in two-dimensional optical lattices, *Phys. Rev. B* 101(1), 014202 (2020)
83. Y. Huang and B. I. Shklovskii, Anderson transition in three-dimensional systems with non-Hermitian disorder, *Phys. Rev. B* 101(1), 014204 (2020)
84. D. W. Zhang, L. Z. Tang, L. J. Lang, H. Yan, and S. L. Zhu, Non-Hermitian topological Anderson insulators, *Sci. China Phys. Mech. Astron.* 63(6), 267062 (2020)
85. J. Claes and T. L. Hughes, Skin effect and winding number in disordered non-Hermitian systems, *Phys. Rev. B* 103(14), L140201 (2021)
86. X. Luo, T. Ohtsuki, and R. Shindou, Universality classes of the Anderson transitions driven by non-Hermitian disorder, *Phys. Rev. Lett.* 126(9), 090402 (2021)
87. X. Luo, T. Ohtsuki, and R. Shindou, Transfer matrix study of the Anderson transition in non-Hermitian systems, *Phys. Rev. B* 104(10), 104203 (2021)
88. K. M. Kim and M. J. Park, Disorder-driven phase transition in the second-order non-Hermitian skin effect, *Phys. Rev. B* 104(12), L121101 (2021)
89. C. C. Wanjura, M. Brunelli, and A. Nunnenkamp, Correspondence between non-Hermitian topology and directional amplification in the presence of disorder, *Phys. Rev. Lett.* 127(21), 213601 (2021)
90. S. Weidemann, M. Kremer, S. Longhi, and A. Szameit, Coexistence of dynamical delocalization and spectral localization through stochastic dissipation, *Nat. Photonics* 15(8), 576 (2021)
91. Q. Lin, T. Li, L. Xiao, K. Wang, W. Yi, and P. Xue, Observation of non-Hermitian topological Anderson insulator in quantum dynamics, *Nat. Commun.* 13(1), 3229 (2022)
92. H. Liu, M. Lu, Z. Q. Zhang, and H. Jiang, Modified generalized Brillouin zone theory with on-site disorder, *Phys. Rev. B* 107(14), 144204 (2023)
93. J. Liu, Z. F. Cai, T. Liu, and Z. Yang, Reentrant non-Hermitian skin effect in coupled non-Hermitian and Hermitian chains with correlated disorder, arXiv: 2311.03777 (2023)
94. C. Wang, W. He, H. Ren, and X. R. Wang, Berezinskii –Kosterlitz–Thouless-like localization–localization transitions in disordered two-dimensional quantized quadrupole insulators, *Phys. Rev. B* 109(2), L020202 (2024)
95. D. Leykam, A. Andreanov, and S. Flach, Artificial flat band systems: from lattice models to experiments, *Adv. Phys. X* 3(1), 1473052 (2018)
96. J. W. Rhim and B. J. Yang, Singular flat bands, *Adv. Phys. X* 6(1), 1901606 (2021)
97. J. Vidal, B. Douçot, R. Mosseri, and P. Butaud, Interaction induced delocalization for two particles in a periodic potential, *Phys. Rev. Lett.* 85(18), 3906 (2000)
98. B. Douçcot and J. Vidal, Pairing of cooper pairs in a fully frustrated Josephson-junction chain, *Phys. Rev. Lett.* 88(22), 227005 (2002)
99. S. Longhi, Aharonov–Bohm photonic cages in waveguide and coupled resonator lattices by synthetic magnetic fields, *Opt. Lett.* 39(20), 5892 (2014)
100. S. Mukherjee, M. Di Liberto, P. Öhberg, R. R. Thomson, and N. Goldman, Experimental observation of Aharonov–Bohm cages in photonic lattices, *Phys. Rev. Lett.* 121(7), 075502 (2018)
101. M. Kremer, I. Petrides, E. Meyer, M. Heinrich, O. Zilberberg, and A. Szameit, A square-root topological insulator with non-quantized indices realized with photonic Aharonov–Bohm cages, *Nat. Commun.* 11(1), 907 (2020)
102. H. Li, Z. Dong, S. Longhi, Q. Liang, D. Xie, and B. Yan, Aharonov–Bohm caging and inverse Anderson transition in ultracold atoms, *Phys. Rev. Lett.* 129(22), 220403 (2022)
103. J. G. C. Martinez, C. S. Chiu, B. M. Smitham, and A. A. Houck, Flat-band localization and interaction-induced delocalization of photons, *Sci. Adv.* 9(50), eadj7195 (2023)
104. J. Vidal, R. Mosseri, and B. Douçcot, Aharonov–Bohm cages in two-dimensional structures, *Phys. Rev. Lett.* 81(26), 5888 (1998)
105. J. Vidal, P. Butaud, B. Dou¸cot, and R. Mosseri, Disorder and interactions in Aharonov–Bohm cages, *Phys. Rev. B* 64(15), 155306 (2001)
106. Y. L. Lin and F. Nori, Quantum interference on the kagomé lattice, *Phys. Rev. B* 50(21), 15953 (1994)
107. Y. L. Lin and F. Nori, Quantum interference in superconducting wire networks and Josephson junction arrays: An analytical approach based on multiple-loop Aharonov–Bohm Feynman path integrals, *Phys. Rev. B* 65(21), 214504 (2002)
108. M. W. Y. Tu, W. M. Zhang, and F. Nori, Coherent

control of double-dot molecules using Aharonov–Bohm magnetic flux, *Phys. Rev. B* 86(19), 195403 (2012)
109. M. Goda, S. Nishino, and H. Matsuda, Inverse Anderson transition caused by flatbands, *Phys. Rev. Lett.* 96(12), 126401 (2006)
110. F. Baboux, L. Ge, T. Jacqmin, M. Biondi, E. Galopin, A. Lemaître, L. Le Gratiet, I. Sagnes, S. Schmidt, H. E. Türeci, A. Amo, and J. Bloch, Bosonic condensation and disorder-induced localization in a flat band, *Phys. Rev. Lett.* 116(6), 066402 (2016)
111. L. Ge, Parity–time symmetry in a flat-band system, *Phys. Rev. A* 92(5), 052103 (2015)
112. H. Ramezani, Non-Hermiticity-induced flat band, *Phys. Rev. A* 96(1), 011802 (2017)
113. D. Leykam, S. Flach, and Y. D. Chong, Flat bands in lattices with non-Hermitian coupling, *Phys. Rev. B* 96(6), 064305 (2017)
114. S. M. Zhang and L. Jin, Flat band in two-dimensional non-Hermitian optical lattices, *Phys. Rev. A* 100(4), 043808 (2019)
115. P. He, H. T. Ding, and S. L. Zhu, Geometry and superfluidity of the flat band in a non-Hermitian optical lattice, *Phys. Rev. A* 103(4), 043329 (2021)
116. T. Biesenthal, M. Kremer, M. Heinrich, and A. Szameit, Experimental realization of PT-symmetric flat bands, *Phys. Rev. Lett.* 123(18), 183601 (2019)
117. B. Qi, L. Zhang, and L. Ge, Defect states emerging from a non-Hermitian flatband of photonic zero modes, *Phys. Rev. Lett.* 120(9), 093901 (2018)
118. S. M. Zhang and L. Jin, Localization in non-Hermitian asymmetric rhombic lattice, *Phys. Rev. Res.* 2(3), 033127 (2020)
119. S. M. Zhang, H. S. Xu, and L. Jin, Tunable Aharonov–Bohm cages through anti-PT-symmetric imaginary couplings, *Phys. Rev. A* 108(2), 023518 (2023)
120. J. Ramya Parkavi and V. K. Chandrasekar, Localization in a non-Hermitian flat band lattice with nonlinearity, *Optik (Stuttg.)* 271, 170129 (2022)
121. S. Ke, W. Wen, D. Zhao, and Y. Wang, Floquet engineering of the non-Hermitian skin effect in photonic waveguide arrays, *Phys. Rev. A* 107(5), 053508 (2023)
122. I. Amelio and N. Goldman, Lasing, quantum geometry and coherence in non-Hermitian flat bands, arXiv: 2308.08418 (2023)
123. C. Martínez-Strasser, M. A. J. Herrera, A. García-Etxarri, G. Palumbo, F. K. Kunst, and D. Bercioux, Topological properties of a non-Hermitian quasi-1D chain with a flat band, *Adv. Quant. Technol.* 7(2), 2300225 (2023)
124. S. Longhi, Inverse Anderson transition in photonic cages, *Opt. Lett.* 46(12), 2872 (2021)
125. P. Molignini, O. Arandes, and E. J. Bergholtz, Anomalous skin effects in disordered systems with a single non-Hermitian impurity, *Phys. Rev. Res.* 5(3), 033058 (2023)
126. T. Hofmann, T. Helbig, C. H. Lee, M. Greiter, and R. Thomale, Chiral voltage propagation and calibration in a topolectrical chern circuit, *Phys. Rev. Lett.* 122(24), 247702 (2019)
127. J. Dong, V. Juričić, and B. Roy, Topolectric circuits: Theory and construction, *Phys. Rev. Res.* 3(2), 023056 (2021)
128. C. H. Lee, S. Imhof, C. Berger, F. Bayer, J. Brehm, L. W. Molenkamp, T. Kiessling, and R. Thomale, Topolectrical circuits, *Commun. Phys.* 1(1), 39 (2018)